# Linear and nonlinear front instabilities in bistable systems

A. Hagberg[a,*], A. Yochelis[b], H. Yizhaq[c], C. Elphick[d], L. Pismen[e], E. Meron[c,f]

[a] *Mathematical Modeling and Analysis, Theoretical Division, Los Alamos National Laboratory, Los Alamos, NM 87545, United States*
[b] *Department of Physics, University of California at Berkeley, Berkeley, CA 94720-7300, United States*
[c] *Department of Solar Energy and Environmental Physics, BIDR, Ben Gurion University, Sede Boker Campus 84990, Israel*
[d] *Centro de Fisica No Lineal y Sistemas Complejos de Santiago, Casilla 17122, Santiago, Chile*
[e] *Department of Chemical Engineering and Minerva Center for Nonlinear Physics of Complex Systems, Technion, Haifa 32000, Israel*
[f] *Department of Physics, Ben-Gurion University, Beer Sheva 84105, Israel*

## Abstract

The stability of planar fronts to transverse perturbations in bistable systems is studied using the Swift–Hohenberg model and an urban population model. Contiguous to the linear transverse instability that has been studied in earlier works, a parameter range is found where planar fronts are linearly stable but nonlinearly unstable; transverse perturbations beyond some critical size grow rather than decay. The nonlinear front instability is a result of the coexistence of stable planar fronts and stable large-amplitude patterns. While the linear transverse instability leads to labyrinthine patterns through fingering and tip splitting, the nonlinear instability often evolves to spatial mixtures of stripe patterns and irregular regions of the uniform states.
© 2006 Elsevier B.V. All rights reserved.

## 1. Introduction

Pattern formation phenomena in bistable systems are determined to a large extent by front instabilities. Fronts which are bi-asymptotic to a pair of stable uniform states can go through transverse instabilities leading to stationary labyrinthine patterns, or through non-equilibrium Ising–Bloch (NIB) bifurcations resulting in traveling wave phenomena such as Bloch spiral waves. The coupling of the two type of instabilities can induce irregular spatio-temporal behaviors ("Bloch-front turbulence") involving recurrent events of vortex-pair nucleation and annihilation. Labyrinthine patterns arising from transverse front instabilities have been observed in the FIS reaction [1] and in the periodically forced oscillatory Belousov–Zhabotinsky (BZ) reaction [2]. The forcing in this case was provided by periodic uniform illumination at a frequency twice as large as the

system's oscillation frequency (2:1 forcing). Bloch spiral waves have been observed in the periodically forced BZ reaction and in liquid crystals [3,4]. Recent experiments on the periodically forced BZ reaction have also demonstrated Bloch-front turbulence [5]. These front instabilities have been found and analyzed in various models including the FitzHugh–Nagumo (FHN) model and a variant of the complex Ginzburg–Landau equation (FCGL) that describes 2:1 periodic forcing of uniform oscillations [6–9].

Another factor affecting pattern formation in bistable systems is the possible pinning of fronts between a pattern and a homogeneous state. Studies of the Swift–Hohenberg (SH) model in one space dimension showed that self-induced pinning, due to the oscillatory shape of the front tails, may prevent a front between a patterned state and a uniform state from propagating [10,11]. The result is that the evolution of a pattern in the SH model might not result in a final state with the lowest free energy.

Bistable systems often arise as a result of symmetry breaking instabilities of uniform states. This is the case with the FHN

---

and the SH models where uniform states lose stability in pitchfork bifurcations. A different case is the FCGL equation for 2:1 forcing. The unforced oscillations appear in a Hopf bifurcation of a stationary uniform solution and correspond to a continuous family of solutions whose phases span the whole circle. The 2:1 forcing induces a pair of saddle-node bifurcations which fix the oscillation phases at two stable values shifted by $\pi$ with respect to one another. Quite often the stationary uniform states, undergoing the zero-wavenumber pitchfork or Hopf bifurcations, go through finite-wavenumber instabilities as well. Resonant coupling of the zero and finite-wavenumber modes can lead to large amplitude patterns [12–15] observed in various systems [16–19].

In this paper we introduce and study another possible outcome of the coupling between zero and finite-wavenumber instabilities — a nonlinear transverse front instability. The asymptotic patterns that develop differ from those developing from linear transverse instabilities in that they often contain regions of uniform states coexisting with stripe domains. We first demonstrate the nonlinear front instability in two different models, the SH equation and a population model [20] (Section 2). We then use the SH equation to study both the linear and nonlinear transverse front instabilities and map them along the bifurcation parameter axis (Section 3). We also find (Section 4) that depinning of a front between a homogeneous state and a pattern occurs via a zigzag instability mechanism, which works far more efficiently than one-dimensional nucleation [10] and greatly reduces the pinning range.

## 2. Numerical demonstrations of linear and nonlinear transverse front instabilities

We consider here two examples of bistable systems, the SH equation and a population model describing urban segregation phenomena [20]. In both models front solutions bi-asymptotic to a symmetric pair of uniform states can become linearly unstable to transverse perturbations. The asymptotic patterns resulting from these linear transverse instabilities are stationary labyrinthine patterns as found in other models such as the FHN and FCGL. Contiguous to these instabilities in parameter space, however, there exist parameter ranges where the fronts are linearly stable but finite-size transverse perturbations still grow. Depending on initial conditions, the asymptotic patterns in this case may look like labyrinths that develop from linear instabilities, or mixtures of stripes and regions of the two uniform states. We demonstrate these behaviors by numerically solving the SH equation and the population model.

### 2.1. The Swift–Hohenberg equation

The SH equation we consider has the form [10,21]

$$u_t = \epsilon u - (\nabla^2 + 1)^2 u - u^3, \tag{1}$$

where $u$ is a real scalar field and $\epsilon$ is the bifurcation control parameter. The zero solution $u = 0$ loses stability to finite-wavenumber perturbations at $\epsilon = 0$, and goes through a
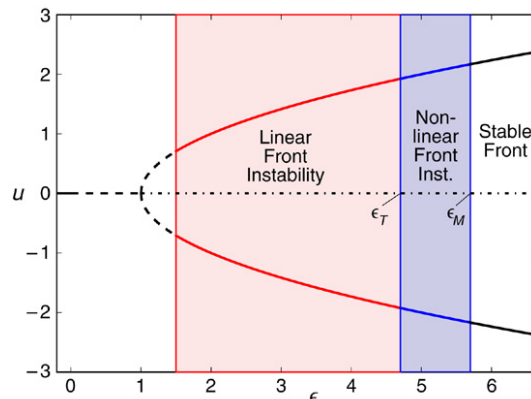


Fig. 1. Bifurcation diagram of uniform solutions to the Swift–Hohenberg Eq. (1). The solution $u = 0$ for $\epsilon < 0$ becomes unstable to finite wavenumber perturbations at $\epsilon = 0$ and then bifurcates to a pair of nonzero unstable solutions at $\epsilon = 1$. At $\epsilon = 1.5$ the two nonzero solutions stabilize but fronts between the two solutions have a linear transverse instability. For $\epsilon \in [\epsilon_T, \epsilon_M]$ fronts are linearly stable to transverse perturbations but large perturbations grow and create a patterned state. Above $\epsilon_M$ the fronts are globally stable.

pitchfork bifurcation at $\epsilon = 1$. The two uniform states, $u_\pm = \pm\sqrt{\epsilon - 1}$, that appear above $\epsilon = 1$ are unstable to finite-wavenumber perturbations but become stable above $\epsilon = 3/2$. Fig. 1 shows a bifurcation diagram of the uniform solutions and the finite-wavenumber instabilities they go through (with additional thresholds to be discussed below).

The bistability of uniform states in the range $\epsilon > 3/2$ allows for front solutions approaching $u_\pm$ asymptotically as $x \to \pm\infty$ or $x \to \mp\infty$. These front solutions are linearly unstable to transverse perturbations up to a threshold $\epsilon = \epsilon_T$ to be calculated in the next section. This linear instability is demonstrated in Fig. 2(a). Beyond $\epsilon_T$, the linear transverse instability disappears; small transverse perturbations of the front decay out as Fig. 2(b) shows. The front, however, remains unstable to finite-size perturbations, implying a *nonlinear* transverse instability. The instability is demonstrated in Fig. 2(c) which also shows the asymptotic pattern that develops — a spatial mixture of parallel stripes and regions of the two stable uniform states. The nonlinear transverse instability disappears at a yet higher threshold, $\epsilon_M$, to be calculated in the next section. Fig. 2(d) demonstrates the global front stability above $\epsilon_M$ by showing the retraction of a pattern state to a planar front.

### 2.2. A population model

The population model we consider here has been introduced and studied in the context of segregation phenomena in residential neighborhoods [20]. It consists of three dynamical variables, $u$, $v$, and $s$, representing, respectively, the densities of two distinct populations and the socio-economic status. A simple version of the model equations, not including non-local migration, is [20]:

$$u_t = u - u^2 + us + \nabla^2 u - \delta_1 \nabla^2 s,$$
$$v_t = \alpha v - v^2 - \beta vs + \delta_2 \nabla^2 v + \delta_3 \nabla^2 s, \tag{2}$$
$$s_t = \epsilon(u - \gamma v - \mu s) - \xi s^3 + \delta_4 \nabla^2 s.$$
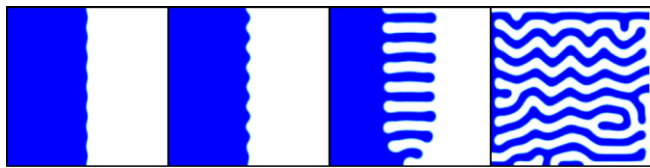
(a) $\epsilon = 2$.
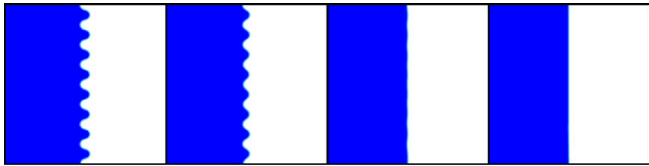


(b) $\epsilon = 5$.
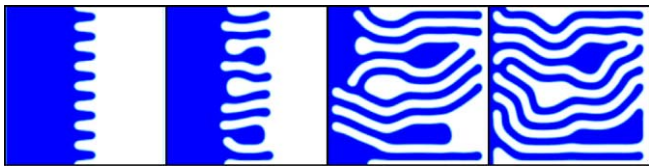


(c) $\epsilon = 5$.
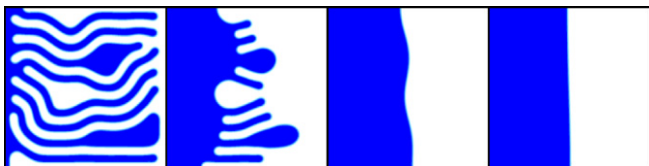


(d) $\epsilon = 7$.

Fig. 2. Numerical solutions of the Swift–Hohenberg Eq. (1) demonstrating the linear and nonlinear front instabilities. (a) In the parameter region of linear front instability small perturbations on a front grow and form a labyrinthine pattern. In the parameter region of nonlinear front instability, (b) small perturbations do not grow, but (c) large perturbations are sufficient to create a patterned state. (d) In the stable parameter range fronts are globally stable. An initial pattern state returns to a front. All frames of SH solutions are of a $64 \times 64$ spatial region with no-flux boundary conditions. Time increases in the frames from left to right [22].

The parameter of interest is $\mu$, the inverse of the segregation strength. Fig. 3 shows a series of bifurcations found in this model in complete analogy to the bifurcations shown in Fig. 1 for the SH model. A symmetric uniform mixed population state, $M = (u_0, v_0, s_0)$, loses stability in a pitchfork bifurcation to a pair of non-symmetric mixed population states, $N_\pm$, as the control parameter, $\mu$, is reduced below $\mu = 2$. This bifurcation is preceded by a Turing bifurcation occurring at $\mu = \mu_c > 2$. The Turing instability is carried over to the two non-symmetric states, $N_\pm$, that appear in the pitchfork bifurcation at $\mu = 2$. The non-symmetric states become stable only below another threshold, $\mu_{nc} < 2$.

Below $\mu = \mu_{nc}$, front solutions bi-asymptotic to the two non-symmetric states, $N_\pm$, are unstable to transverse perturbations and evolve to labyrinthine patterns. Below another
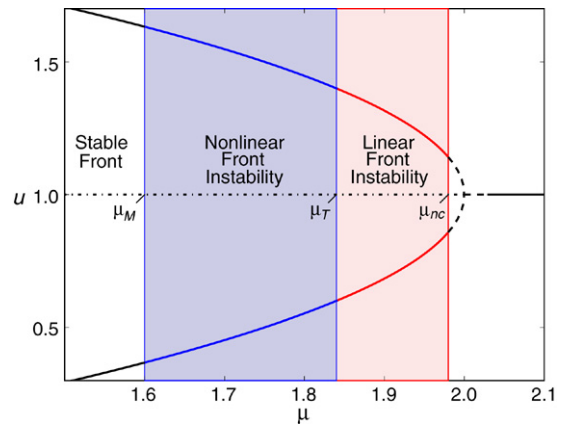


Fig. 3. Bifurcation diagram for solutions to the $u$ field of the urban population model (2). The symmetric mixed population state $M = (u_0, v_0, s_0)$ becomes unstable to finite wavenumber perturbations below $\mu = \mu_c \approx 2.029$. At $\mu = 2$ it bifurcates to a pair of asymmetric mixed population states, $N_\pm$. These solutions are unstable to finite wavenumber perturbations, but become linearly stable below $\mu = \mu_{nc} \approx 1.98$. In this parameter range the system is bistable and admits front solutions bi-asymptotic to $N_\pm$. These solutions, however, are linearly unstable to transverse perturbations down to $\mu = \mu_T \approx 1.84$. Below $\mu_T$ the front solutions are linearly stable to transverse perturbations but are unstable to finite size (nonlinear) perturbations until $\mu = \mu_M \approx 1.6$. Parameters: $\mu = 1.75$, $\delta_4 = 0.1$, $\delta = 1.12$; all the other parameters are equal to 1.
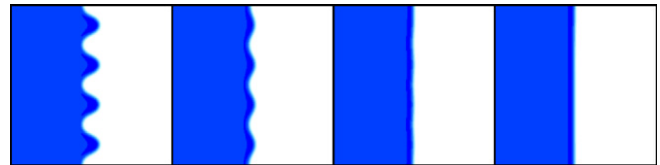


(a) $\mu = 1.75$.
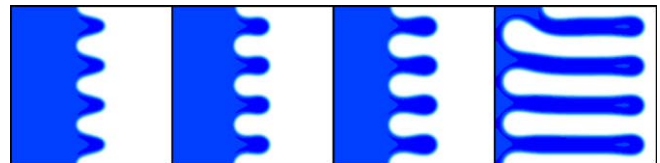


(b) $\mu = 1.75$.

Fig. 4. Nonlinear instability in urban population model. (a) A small perturbation retracts to a planar front. (b) A large perturbation grows into a patterned state. All images are of a $50 \times 50$ region with no-flux boundary conditions. Time increases in the frames from left to right. Parameters in Eq. (2): $\mu = 1.75$, $\delta_4 = 0.1$, $\delta = 1.12$; all the other parameters are equal to 1.

threshold, $\mu_T$ [23], the fronts become linearly stable but finite size perturbations do grow, indicating the existence of a nonlinear front instability. Below yet another threshold, $\mu_M \approx 1.6$, the nonlinear front instability disappears. Fig. 4 demonstrates the nonlinear front instability for $\mu_M < \mu < \mu_T$.

## 3. Mapping the front instabilities in parameter space

We evaluate the parameter ranges of the linear and nonlinear front instabilities using the SH model which is simpler to

analyze. The population model behaves qualitatively in the same way.

### 3.1. The linear transverse front instability

Front solutions bi-asymptotic to the two stable states, $u_\pm$, exist for $\epsilon > 3/2$, but are linearly unstable to transverse perturbations as long as $\epsilon$ is smaller than some threshold value $\epsilon_T$. We evaluate now this threshold.

Denoting the unstable planar front solution by $I(x)$ we write a more general solution as

$$u(x, y, t) = I[x - \Lambda(Y, T_1, T_2, \ldots)] + \lambda u_1 + \lambda^2 u_2 + \cdots, \quad (3)$$

where $x = \Lambda$ is the front position, $\lambda \ll 1$ is a small auxiliary parameter, $Y = \sqrt{\lambda} y$ is a weakly varying transverse coordinate, and $T_n = \lambda^n t$ are slow multiple time variables. Since we are interested in deriving the threshold, $\epsilon_T$, for the linear transverse instability, we will assume that $\Lambda$ is small and neglect nonlinear terms in $\Lambda$. Substitution of Eq. (3) in Eq. (1) yields at order $\lambda$:

$$\mathcal{L}u_1 = -\Lambda_{T_1} I' - 2(I' + I''')\Lambda_{YY} \equiv J_1, \quad (4)$$

where $\mathcal{L} = \epsilon - 3I^2 - (\partial_x^2 + 1)^2$. Solvability of Eq. (4) requires $\langle J_1, I' \rangle = 0$ or

$$\Lambda_{T_1} = 2(D_1 - 1)\Lambda_{YY}, \quad (5a)$$

where

$$D_1 = \frac{\langle I'', I'' \rangle}{\langle I', I' \rangle} = \frac{\int_{-\infty}^{\infty}(I'')^2 dx}{\int_{-\infty}^{\infty}(I')^2 dx}. \quad (5b)$$

In obtaining Eq. (5b) we used the front symmetry $I(-x) = -I(x)$. Using Eq. (5a) in Eq. (4) we find the following form for $u_1$

$$u_1 = \Lambda_{YY} f(x - \Lambda), \quad (6)$$

where $f$ is a solution of

$$\mathcal{L}f = -2D_1 I' - 2I'''. \quad (7)$$

Proceeding to order $\lambda^2$ we find

$$\mathcal{L}u_2 = -\Lambda_{T_2} I' - (I' + 2D_1 f + 2f'')\Lambda_{YYYY} \equiv J_2. \quad (8)$$

Solvability of Eq. (8) requires $\langle J_2, I' \rangle = 0$ or

$$\Lambda_{T_2} = (2D_2 - 1)\Lambda_{YYYY}, \quad (9a)$$

where

$$D_2 = \frac{\langle D_1 f + f'', I' \rangle}{\langle I', I' \rangle} = \frac{\langle D_1 I' + I''', f \rangle}{\langle I', I' \rangle}. \quad (9b)$$

Inserting Eqs. (5a) and (9a) into $\Lambda_t = \lambda \Lambda_{T_1} + \lambda^2 \Lambda_{T_2}$ and rescaling back to the fast variables $t$ and $y$ we obtain the evolution equation for the front position,

$$\Lambda_t = 2(D_1 - 1)\Lambda_{yy} + (2D_2 - 1)\Lambda_{yyyy}. \quad (10)$$

According to Eq. (10), the growth rate of transverse front perturbations $\Lambda = \Lambda_0 \exp(\sigma_f t + iky)$ is given by the dispersion relation

$$\sigma_f(k) = -2(D_1 - 1)k^2 + (2D_2 - 1)k^4. \quad (11)$$
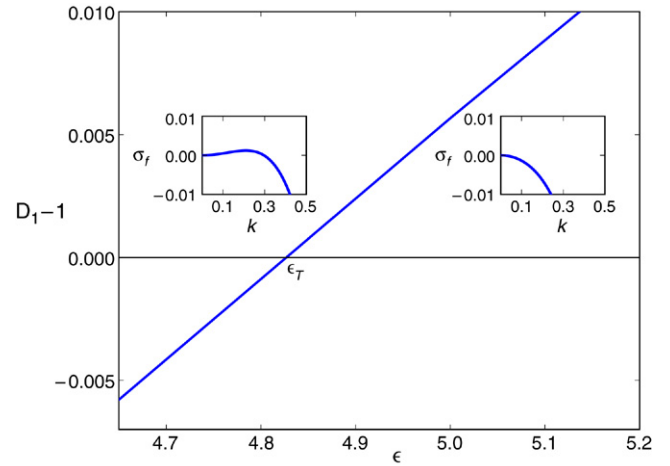


Fig. 5. A graph of $D_1 - 1$ vs. the control parameter $\epsilon$. The zero of $D_1 - 1$ denotes the onset, $\epsilon_T$, of the linear transverse front instability. The insets show dispersion relations for transverse modes in the unstable ($\epsilon < \epsilon_T$) and stable ($\epsilon > \epsilon_T$) regimes.

The coefficients $D_1$ and $D_2$, given by Eqs. (5b) and (9b) respectively, have been calculated numerically. Fig. 5 shows the dependence of $D_1$ on the control parameter $\epsilon$. The onset of the linear transverse instability occurs when $D_1(\epsilon) = 1$ which gives the value $\epsilon_T \approx 4.825$. Below $\epsilon_T$ (for which $D_1 < 1$) the front is linearly unstable to wavenumbers within the band $0 < |k| < \sqrt{2(1 - D_1)/(1 - 2D_2)}$. The fastest growing mode is given by $|k| = (1 - D_1)/(1 - 2D_2)$ (numerical calculations of $D_2$ in the range $3/2 < \epsilon < \epsilon_T$ yield positive values for $1 - 2D_2$). Graphs of the dispersion relation (11) below and above $\epsilon_T$ are given in the insets of Fig. 5.

### 3.2. The nonlinear transverse front instability

Above $\epsilon_T$ the front is linearly stable but nonlinearly unstable as Fig. 2(b),(c) demonstrate. The nonlinear instability follows from the coexistence of stable planar fronts and stable large-amplitude patterns. A prerequisite for that is coexistence of the stable symmetric uniform states, $u_\pm$, with stable large-amplitude patterns. Such coexistence can result from the resonant coupling of the finite-wavenumber mode, associated with the instability of the $u = 0$ state at $\epsilon = 0$, and the zero-wavenumber mode, associated with the pitchfork bifurcation at $\epsilon = 1$ [12–14]. The growth of both modes for $\epsilon > 1$ is shown by the dispersion relation displayed in Fig. 6.

In the range $1 < \epsilon < 3/2$ large-amplitude patterns appear to be the only attractor of the system. The symmetric uniform states, $u_\pm$, are unstable in this range, and the finite-wavenumber modes that grow do not saturate at small amplitudes, but rather grow to form large-amplitude patterns spanning the whole range between $u_+$ and $u_-$. The large-amplitude patterns persist beyond $\epsilon = 3/2$, where the symmetric uniform states, $u_\pm$, become stable and, as Fig. 7 demonstrates, also beyond $\epsilon = \epsilon_T$, where the front solutions that asymptote to $u_\pm$ become linearly stable [24].

The nonlinear front instability that appears at $\epsilon_T$ persists up to a second threshold $\epsilon_M$, beyond which arbitrarily large
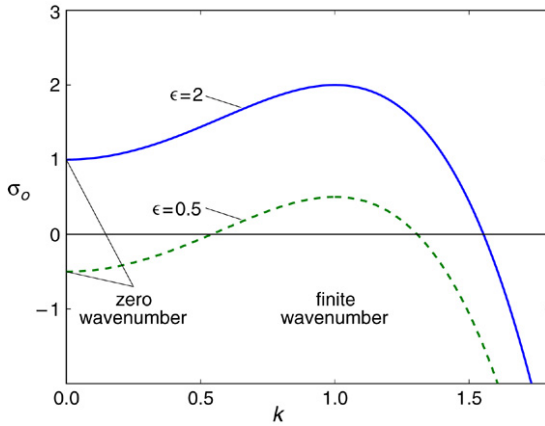
Fig. 6. Example dispersion relations for the $u = 0$ solution of the Swift–Hohenberg model, $\sigma_o = \epsilon - (1 - k^2)^2$, calculated for $\epsilon = 0.5$ (dashed curve) and $\epsilon = 2$ (solid curve). For $\epsilon = 0.5$ the $u = 0$ solution is unstable to finite wavenumber perturbations. For $\epsilon > 1$ it is unstable to finite-wavenumber and zero-wavenumber perturbations.
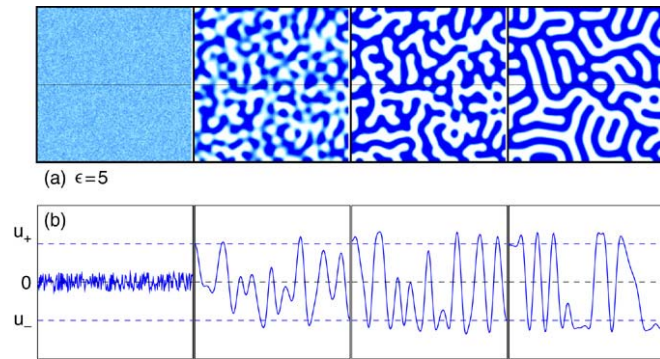


Fig. 7. Development of labyrinthine pattern from random initial conditions. (a) The spatial pattern evolves quickly into a labyrinth. (b) A cross section of the pattern (at the position indicated in (a) by the horizontal line) shows that the labyrinthine pattern is a large-amplitude pattern which approaches the value of the uniform states $u_\pm$. Parameters: $\epsilon = 5$, $u_\pm = \sqrt{\epsilon - 1} = 2$, $x = y = [0, 64]$, $t = 0, 1, 2, 480$.

perturbations decay in time as Fig. 2(d) demonstrates. To evaluate $\epsilon_M$ we consider front solutions that are bi-asymptotic to one of the two uniform states, $u_\pm$, and to a pattern state with stripes oriented perpendicularly to the front line. We identify the threshold $\epsilon_M$ with the $\epsilon$ value at which neither state invades the other, that is, the front solution is stationary. Fig. 8 shows numerical solutions of the SH equation suggesting the existence of a unique value, $\epsilon_M \approx 5.7$, at which the front separating a uniform state and a pattern state, with stripes perpendicular to the front line, is stationary. Below that value, $\epsilon < \epsilon_M$, the pattern state invades the uniform state [Fig. 8(a)] and, consequently, large enough perturbations of a planar front, that locally converge to the pattern state, will grow. Above $\epsilon_M$ the uniform state invades the pattern state [Fig. 8(b)] and front perturbations of arbitrary size decay.

The value of $\epsilon_M$ can also be calculated using the fact that the SH model is a gradient system having a Lyapunov or energy
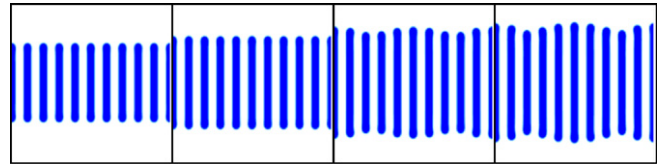


(a) $\epsilon = 5.65$.
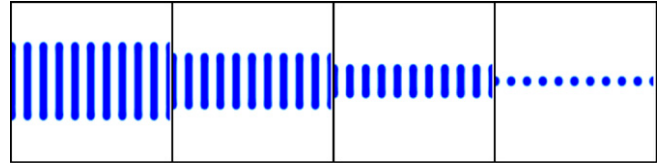


(b) $\epsilon = 5.75$.

Fig. 8. Numerical solutions of the SH equation with a uniform state and pattern state in the same domain. The nonlinear front instability boundary $\epsilon_M \approx 5.7$ can be estimated by finding the value of $\epsilon$ where the interface between the uniform and pattern state is stationary. (a) For $\epsilon < \epsilon_M$, the pattern state invades the uniform state. (b) For $\epsilon > \epsilon_M$, the uniform state invades the pattern state. Parameters: $x = y = [0, 65.5]$. The wavelength of the stripe pattern is $k \approx 0.96$. Time increases in the frames from left to right.

functional

$$\mathcal{F}(u) = \int d\mathbf{r} \left[ -\frac{\epsilon}{2} u^2 + \frac{1}{4} u^4 + \frac{1}{2} \left( \nabla^2 u + u \right)^2 \right], \qquad (12)$$

satisfying $\dot{\mathcal{F}} = -\int d\mathbf{r} \, (\delta \mathcal{F}/\delta u)^2 \leq 0$. The value of $\epsilon_M$ is determined by requiring the energy of the pattern state to be equal to that of the uniform state. Such a calculation has been previously done but not with good accuracy; in Ref. [25] the energy is estimated from two-dimensional numerical solutions ($\epsilon_M \approx 6.3$) and in Ref. [10] by numerically solving a stationary, one-dimensional version of Eq. (1) ($\epsilon_M \approx 6.287$). We calculated the energy of a stripe pattern by numerically solving a one-dimensional version of the SH equation (1) and Eq. (12). The energies of pattern and uniform solutions, shown in Fig. 9, are equal at $\epsilon_M \approx 5.7$ where the minimum energy stripe pattern has wavenumber $k \approx 0.96$. This is consistent with our observations of the interface propagation between the stripe and uniform states shown in Fig. 8.

## 4. Pinning of front motion

Estimating $\epsilon_M$ by energy considerations is not applicable when the front motion is pinned by the periodic structure of the pattern state. Pinning effects have indeed been found in the one-dimensional SH model [10,11]; the pattern state does not invade the uniform states in the range $\epsilon_P < \epsilon < \epsilon_M$, where $\epsilon_P \approx 1.7574$, despite the lower energy of the pattern state. In two space dimensions no pinning can occur, unless the stripes are parallel to the front line. In that case, which imitates the one-dimensional setup, we found a reduced pinning range, $\epsilon_{DP} < \epsilon < \epsilon_M$ where $\epsilon_{DP} > \epsilon_P$ is rather close to the linear instability limit $\epsilon_T$. The depinning mechanism via nucleation of new stripes of the pattern state, which operates in one dimension, turns out to be ineffective in a two-dimensional
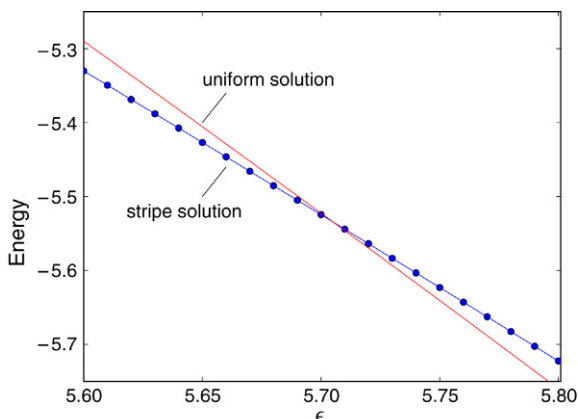
Fig. 9. The energy of solutions to the SH equation for a spatially uniform solution, $(\epsilon - 1)^2/4$, and for a stripe pattern with wavenumber $k \approx 0.96$. The stripe pattern has lower energy for $\epsilon < \epsilon_M \approx 5.7$. The energy of the stripe pattern is computed by solving the one-dimensional version of Eq. (1) for a periodic stripe pattern and evaluating the Lyapunov functional (12). The pattern with wavenumber $k \approx 0.96$ is the minimum energy pattern in this range of $\epsilon$. The energy values are normalized to unit area.
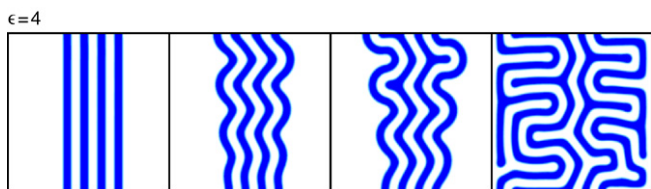


Fig. 10. Depinning of the pattern state in the SH equation. In a one dimensional system the stripe pattern is stationary (pinned). In two dimensions the zigzag instability causes depinning of the stripes. The wavelength of the zigzag instability is somewhat larger than that of the stripe pattern. The pattern evolves into a labyrinth by nucleating convex–concave disclination pairs. Parameters: $\epsilon = 4$, $x = y = [0, 64]$, $t = 0, 950, 1150, 2450$.

setting. The mechanism of depinning in the range $\epsilon_P < \epsilon < \epsilon_{DP}$ is shown in Fig. 10. It consists of a zigzag instability of the pattern states followed by the nucleation of convex–concave disclination pairs [26] with the convex disclinations moving toward the uniform states as the pattern spreads out. The parameter range of pinning shrinks considerably due to the more effective two-dimensional depinning.

## 5. Discussion

We considered here front solutions which are bi-asymptotic to pairs of stable, symmetric uniform states, and studied their stability to transverse perturbations using the SH equation and a population model. We demonstrated in both models the existence of a nonlinear transverse front instability whereby small transverse perturbations along the front line decay while perturbations beyond some critical amplitude grow and evolve towards a stationary pattern state. The following conditions appear necessary for a nonlinear transverse front instability to occur: (i) coexistence of a stable planar front and a stable large-amplitude stripe pattern, and (ii) dominance of the pattern state over the uniform states (pattern state invades the uniform states).

Condition (i) requires the coexistence of a stable large-amplitude pattern with a symmetric pair of stable uniform states (e.g. $u_\pm$ in the SH model). Such state coexistence can result from resonant coupling of zero and finite-wavenumber modes [12,14]. Dispersion relations which show the growth of both modes, as in Fig. 6, may therefore serve as indicators for the possible coexistence of large-amplitude patterns and uniform states. Our numerical studies show that both the FHN and FCGL models have a parameter range where the dispersion relations of the trivial states are as in Fig. 6, and that in this range large-amplitude patterns indeed coexist with the symmetric pairs of uniform states. In the case of the FHN model, however, condition (i) is not satisfied as planar fronts in this range appear to be linearly unstable. In the range where planar fronts are linearly stable the dispersion relation shows a maximum at $k = 0$. The pattern states that develop consists of large coarsening domains of the two uniform states, and condition (i) is again not satisfied. Indeed our attempts to identify a nonlinear front instability in the FHN model have not succeeded. Our studies of the FCGL equation are less conclusive and further studies exploring wider parameter ranges are needed.

Condition (ii) can be violated by pinning effects which render the fronts (separating the pattern state and the uniform states) stationary over some parameter ranges. This is the case with the SH model in one space dimension [10]. Our two-dimensional studies of the SH model do not reveal pinning effects when the stripes are perpendicular to the front line.

The asymptotic patterns that develop from nonlinear transverse front instabilities can differ considerably from the labyrinthine patterns that develop from linear front instabilities. The linear stability of the fronts along with the stability of the symmetric uniform states often favor the formation of uniform solution regions intermingled with stripes, as Fig. 2(c) (rightmost frame) shows. In this particular simulation the uniform solution regions result from a significant mismatch between the wavenumber of the transverse front perturbation and the wavenumber of the stripe pattern. The results of this study may be relevant to observations of oscillation-phase interfaces in vibrated granular layers [27,28].

## References

[1] K.J. Lee, H.L. Swinney, Lamellar structures and self-replicating spots in a reaction–diffusion system, Phys. Rev. E 51 (1995) 1899.
[2] A. Yochelis, A. Hagberg, E. Meron, A.L. Lin, H.L. Swinney, Development of standing-wave labyrinthine patterns, SIADS 1 (2) (2002) 236–247.

[3] S. Nasuno, N. Yoshimo, S. Kai, Structural transition and motion of domain walls in liquid crystals under a rotating magnetic field, Phys. Rev. E 51 (1995) 1598.

[4] T. Frisch, J.M. Gilli, Excitability and defect-mediated turbulence in nematic liquid crystal, J. Phys. II France 5 (1995) 561–572.

[5] B. Marts, A. Hagberg, E. Meron, A.L. Lin, Bloch-front turbulence in a periodically forced Belousov–Zhabotinsky reaction, Phys. Rev. Lett. 93 (2004) 108305.

[6] P. Coullet, K. Emilsson, Strong resonances of spatially distributed oscillators: A laboratory to study patterns and defects, Physica D 61 (1992) 119–131.

[7] M. Bode, A. Reuter, R. Schmeling, H.-G. Purwins, Measurement of the transition from uni-to-bi-directional front propagation in a reaction–diffusion system, Phys. Lett. A 185 (1994) 70.

[8] A. Hagberg, E. Meron, From labyrinthine patterns to spiral turbulence, Phys. Rev. Lett. 72 (15) (1994) 2494–2497.

[9] A. Hagberg, E. Meron, Complex patterns in reaction–diffusion systems: A tale of two front instabilities, Chaos 4 (3) (1994) 477–484.

[10] I.S. Aranson, B.A. Malomed, L.M. Pismen, L.S. Tsimring, Crystallization kinetics and self-induced pinning in cellular patterns, Phys. Rev. E 62 (2000) R5–R8.

[11] P. Coullet, C. Riera, C. Tresser, Stable static localized structures in one dimension, Phys. Rev. Lett. 84 (2000) 3069–3072.

[12] G. Dewel, S. Métens, M'F. Hilali, P. Borckmans, C.B. Price, Resonant patterns through coupling with a zero mode, Phys. Rev. Lett. 74 (1995) 4647–4650.

[13] M'F Hilali, G. Dewel, P. Borckmans, Subharmonic and strong resonances through coupling with a zero mode, Phys. Lett. A 217 (1996) 263–268.

[14] S. Métens, G. Dewel, P. Borckmans, R. Engelhardt, Pattern selection in bistable reaction–diffusion systems, Europhys. Lett. 37 (1997) 109.

[15] A. Yochelis, C. Elphick, A. Hagberg, E. Meron, Frequency locking in extended systems: The impact of a Turing mode, Europhys. Lett. 69 (2005) 170–176.

[16] W.J. Firth, A.J. Scroggie, G.S. McDonald, Hexagonal patterns in optical bistability, Phys. Rev. A 46 (1992) R3609–R3612.

[17] G. Ahlers, L.I. Berge, D.S. Cannell, Thermal convection in the presence of a first-order phase change, Phys. Rev. Lett 70 (1993) 2399–2402.

[18] T. Ackemann, Y.A. Logvin, A. Heuer, W. Lange, Transition between positive and negative hexagons in optical pattern formation, Phys. Rev. Lett. 75 (1995) 3450–3453.

[19] W. Breazeal, K.M. Flynn, E.G. Gwinn, Static and dynamic two-dimensional patterns in self-extinguishing discharge avalanches, Phys. Rev. E 52 (1995) 1503–1515.

[20] H. Yizhaq, B.A. Portnov, E. Meron, A mathematical model of segregation patterns in residential neighbourhoods, Environ. Planning A 36 (2004) 149–173.

[21] T. Passot, A.C. Newell, Towards a universal theory for natural patterns, Physica D 74 (1994) 301–352.

[22] Supplemental material can be found at http://math.lanl.gov/nonlinearfront/.

[23] H. Yizhaq, Population dynamics: Urban segregation as a nonlinear phenomenon, Ph.D. Thesis, Ben Gurion University, 2003.

[24] Note that the linear stability of front solutions beyond $\epsilon_T$ excludes the interpretation of the large amplitude patterns above $\epsilon_T$ as resulting from fingering and tip-splitting processes that follow a linear transverse front instability [8].

[25] K. Ouchi, H. Fujisaka, Phase ordering kinetics in the Swift–Hohenberg equation, Phys. Rev. E 54 (1996) 3895–3898.

[26] A.C. Newell, T. Passot, N. Ercolani, R. Indik, Elementary and composite defects of striped patterns, J. Phys. II France 5 (1995) 1863–1882.

[27] P.B. Umbanhowar, F. Melo, H.L. Swinney, Periodic, aperiodic, and transient patterns in vibrated granular layers, Physica A 249 (1998) 1–9.

[28] I.S. Aranson, D. Blair, W.K. Kwok, G. Karapetrov, U. Welp, G.W. Crabtree, V.M. Vinokur, L.S. Tsimring, Controlled dynamics of interfaces in a vibrated granular layer, Phys. Rev. Lett. 82 (4) (1999) 731–734.